frontiers in Materials

ORIGINAL RESEARCH
published: 07 June 2019
doi: 10.3389/fmats.2019.00122

Highly Sensitive and Selective Ethanol Sensor Based on ZnO Nanorod on SnO_2 Thin Film Fabricated by Spray Pyrolysis

T. Tharsika[1], M. Thanihaichelvan[2], A. S. M. A. Haseeb[3]* and S. A. Akbar[4]*

[1] Department of Interdisciplinary Studies, Faculty of Engineering, University of Jaffna, Kilinochchi, Sri Lanka, [2] Department of Physics, Faculty of Science, University of Jaffna, Jaffna, Sri Lanka, [3] Department of Mechanical Engineering, Faculty of Engineering, University of Malaya, Kuala Lumpur, Malaysia, [4] Department of Materials Science and Engineering, Center for Industrial Sensors and Measurements, Ohio State University, Columbus, OH, United States

This work reports the fabrication of mixed structure of ZnO nanorod on SnO_2 thin film via spray pyrolysis followed by thermal annealing and their gas sensing properties. ZnO/SnO_2 nanostructures are successfully prepared on a gold interdigitated alumina substrate by spraying varying mixed precursor concentrations of zinc acetate and tin (IV) chloride pentahydrate solutions in ethanol and thermal annealing. The morphology of the nanostructures is controlled by tailoring the Zn:Sn ratio in the precursor solution mixture. Unique ZnO crystals and ZnO nanorods are observed under a field emission scanning electron microscopy (FESEM) when the Zn/Sn ratio in the precursor solution is in between 13:7 and 17:3 after thermal annealing. The fabricated nanostructures are tested for ethanol, methane and hydrogen in air ambient for various gas concentrations ranging from 25 to 400 ppm and the effect of fabrication conditions on the sensitivity and selectivity are studied. Among the nanostructure sensors studied, the film fabricated with molar ratio of Zn/Sn =3:1 shows better sensitivity and selectivity to ethanol due to high sensing surface area of the nanorod. The response to 25 ppm ethanol is found to be as high as 50 at an operating temperature of 400°C.

Keywords: spray pyrolysis, ZnO, nanorod, SnO_2, thin film, gas sensor, ethanol, nanocomposite

OPEN ACCESS

Edited by:
Kalisadhan Mukherjee, Pandit Deendayal Petroleum University, India

Reviewed by:
Dr. Subhasis Roy, University of Calcutta, India
Sudip Mondal, Pukyong National University, South Korea

****Correspondence:***
T. Tharsika
tharsika@eng.jfn.ac.lk
A. S. M. A. Haseeb
haseeb@um.edu.my

Specialty section:
This article was submitted to Functional Ceramics, a section of the journal Frontiers in Materials

Received: *25 January 2019*
Accepted: *13 May 2019*
Published: *07 June 2019*

Citation:
Tharsika T, Thanihaichelvan M, Haseeb ASMA and Akbar SA (2019) Highly Sensitive and Selective Ethanol Sensor Based on ZnO Nanorod on SnO_2 Thin Film Fabricated by Spray Pyrolysis. Front. Mater. 6:122. doi: 10.3389/fmats.2019.00122

INTRODUCTION

Gas sensors based on metal oxide nanostructures have been widely studied and used in applications ranging from health and safety to emission control (Comini et al., 2002; Lin et al., 2015; Yao et al., 2016; Kwak et al., 2018; Liu et al., 2019a). These sensors are attractive because of their high sensitivity, low cost, simplicity and compatibility with modern electronic devices due to direct electrical readouts (Miller et al., 2014). Until now, several metal oxides including TiO_2, In_2O_3, WO_3, ZnO, TeO_2, CuO, SnO_2, and NiO are used in resistive-type metal oxide gas sensors (Dey, 2018). However, these single metal oxide gas sensors generally have the disadvantage of low sensitivity, high operating temperature, and poor selectivity between gases (Arafat et al., 2014).

Ethanol sensors are being used in numerous applications, such as, to monitor chemical reactions, breath analysis, biomedical productions, and quality control of foods (Kolmakov et al., 2003; Timmer et al., 2005). Augmented usage of ethanol increases the issues of explosion hazards

(Powers et al., 2001) and ground-water pollution (Freitas et al., 2010). Lower selectivity is one of the major drawbacks of the metal oxide-based sensors for selective ethanol sensing applications. Several approaches have been used to improve the sensitivity and selectivity of single metal oxide-based ethanol sensor. These include addition of noble metals (Chen et al., 2019; Liu et al., 2019b; ul Haq et al., 2019) doping of metal oxide catalyst (Park et al., 2015; NaderiNasrabadi et al., 2016; Lupan et al., 2017; Tan et al., 2018), developing composite metal oxides consisting of binary or ternary phase metal oxide systems (Li et al., 2019; Wang et al., 2019) and development of nanostructures with different morphologies (Drobek et al., 2016; Wang et al., 2018; Yang et al., 2018). Among the approaches used, tailoring of composite metal oxides with different morphologies presents a good potential for tuning the sensitivity and selectivity during gas sensing. Many recent studies have shown that the selectivity and operating temperature of resistive-type gas sensors can be improved through the use of composite metal oxides (Andre et al., 2019; He et al., 2019; Rong et al., 2019; Sakthivel and Nammalvar, 2019).

The composite nanostructures of ZnO and SnO_2 received special attention due to their unique electronic properties that are keys for selective gas sensing. Stoichiometric nature of each varies significantly and that leads to increase gas sensing potential of the composite material. Generally SnO_2 has non-stoichiometric nature below the substrate temperature of 450°C in spray pyrolysis process (Amma et al., 2005), while ZnO has defects in structure (Demir-Cakan et al., 2008). Due to this behavior, chemisorption of oxygen is high on ZnO than on SnO_2. SnO_2 also enhances the desorption process in ZnO-nanorod/SnO_2-thinfilm gas sensors by transferring electron from SnO_2 to ZnO due to the lower work function of the latter (Lu et al., 2012; Park et al., 2013).

ZnO/SnO_2 based nanostructures have been mostly synthesized by a two-step fabrication process (Cheng et al., 2009; Pan et al., 2012; Park et al., 2013), and extensively used in various applications such as, transparent electrode, photovoltaic, light emitting diodes, field emission transistor and energy harvesting due to their great potential properties (Wang and Rogach, 2014; Rong et al., 2019). In our previous studies (Tharsika et al., 2014a,b), we reported on the fabrication of ZnO-SnO_2 thin films by spray pyrolysis on glass substrate and studied the structural and optical properties of the films. We observed the formation of ZnO nanorods for films sprayed with Zn/Sn = 3:1 followed by thermal annealing at 350°C and reported as short communication (Tharsika et al., 2015).

In this study, we investigate the role of Zn:Sn molar ratio on the morphology of the nanostructures fabricated by the same spray pyrolysis and thermal annealing method. A wide range of precursor mixtures (Zn/Sn = 13:7, 14:6, 15:5, 16:4, and 17:3) are tested and the aspect ratio of ZnO nanorod is investigated in detail. We also fabricate solid state gas sensors using the composite films on gold interdigitated alumina substrate and their gas sensing properties toward number of reducing gases such as, ethanol, methane and hydrogen are studied. The selectivity toward ethanol for the ZnO/SnO_2 composite sensor is studied for various molar ratio of the precursor solution. A possible mechanism for the improved selectivity along with higher sensitivity for 15Z5S nanostructure sensor is suggested.

MATERIALS AND METHODS

Fabrication of ZnO/SnO_2 Nanostructures

ZnO/SnO_2 nanostructures were deposited by spray pyrolysis on gold interdigitated alumina substrates using zinc acetate ($Zn(C_2H_3O_2)_2$) [98% purity, Sigma Aldrich-USA] and tin (IV) chloride pentahydrate ($SnCl_4.5H_2O$) [99.99% trace metals basis, Sigma Aldrich-USA] solutions in absolute ethanol. The detailed procedure was reported elsewhere (Tharsika et al., 2014b). Briefly, the mixed precursor solutions were obtained by adding proportional volumes of equimolar $Zn(C_2H_3O_2)_2$ and $SnCl_4.5H_2O$ solutions in ethanol with the volume ratios of 13:7, 14:6, 15:5, 16:4, and 17:3. The mixed solution was ultrasonicated for a minute and directly sprayed onto the substrate by a spray gun using dry nitrogen as the carrier gas. The substrate temperature was maintained at 350°C throughout the spraying process and the number of spray was kept as constant at 180 for all the samples. Finally, the sprayed films were annealed at 350°C for 1 h. The designation of the deposited films is given in **Table 1**. For comparison of gas sensing characteristics, ZnO and SnO_2 thin films were also fabricated.

Characterizations of Nanostructures

X-ray diffraction patterns of ZnO/SnO_2 nanostructures before and after annealing were determined using X-ray diffractometer (XRD: Siemen D-5000 model) with a monochromatic CuKα radiation (λ = 0.15406 nm) and a Ni filter. The current and voltage were 40 mA and 40 kV, respectively. The data were collected in the range of 20–80° (2θ), with a scanning step of 0.05°/s. The surface morphology of the films was investigated by using a field-emission scanning electron microscopy (FESEM: Auriga Zeiss Ultra-60). Elemental composition was obtained at two different places including on the nanorod and on the surface of the underlying film using FESEM coupled with an energy dispersive X-ray spectroscopy (EDX) with applied beam voltage of 20 keV.

TABLE 1 | Volume of Zn and Sn ion in mixed precursor solution for different thin films.

Film designation	Volume in mixed precursor solution (ml)	
	$Zn(C_2H_3O_2)_2$	$SnCl_4.5H_2O$
13Z7S	13	7
14Z6S	14	6
15Z5S	15	5
16Z4S	16	4
17Z3S	17	3

Gas Sensing Measurements

The fabricated nanostructures on printed Au interdigitated alumina substrates were directly used as a gas sensor for sensing measurements. The distance between the adjacent Au fringes and fringe width were 200 and 100 μm, respectively. A gold wire (99.9% metal basis) with a diameter of 0.2 mm was jointed to Au interdigitated electrode using conducting Au paste to make the electrical connection between electrode and gold wire.

The sensor was placed inside a horizontal tube furnace, and sensing measurements were carried out for various target gases such as ethanol, methane and hydrogen. The concentration of the gases (25, 50, 100, 200, and 400 ppm) was controlled by a digital mass flow controller. A mixture of 80% of nitrogen and 20% of oxygen was used as the ambient to simulate the air atmosphere inside the furnace. Measurements were done by using a computer-controlled data acquisition system. The resistance in air (R_a) and in the presence of the test gases (R_g) were recorded, and the sensitivity of the sensor was calculated as R_a/R_g.

RESULTS AND DISCUSSION

Morphological Studies

Figure 1 shows the FESEM images of ZnO/SnO_2 nanostructures sprayed with different Zn:Sn molar ratio in the precursor solution of 13:7, 14:6, 15:5, 16:4, and 17:3 on alumina substrates before and after thermal annealing. As seen in **Figures 1A–E**, all as-sprayed films show flake like structures on the surface and no evidences for nanorods or other nanostructures are found.

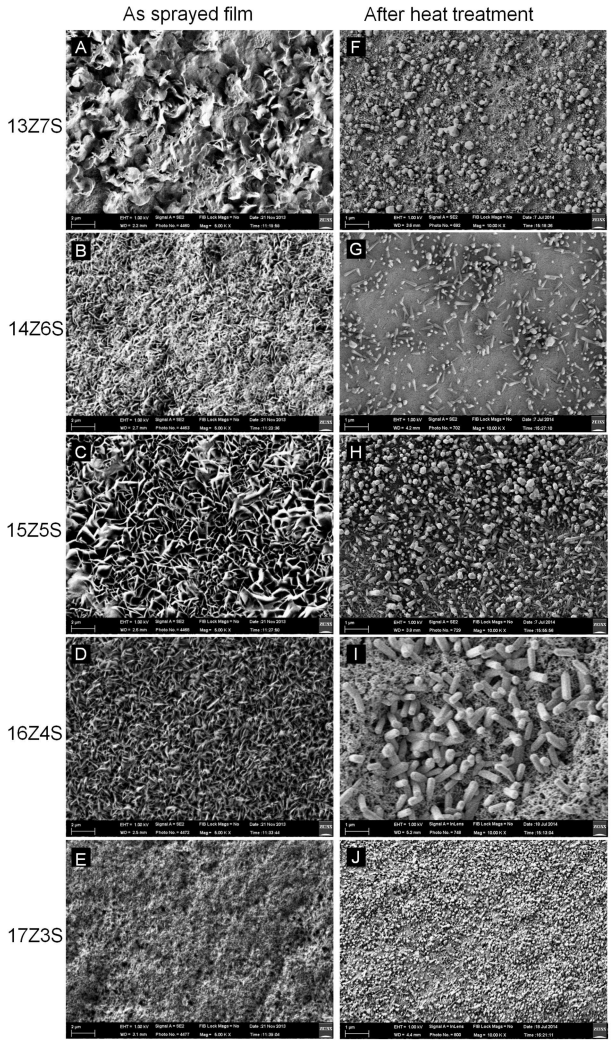

FIGURE 1 | FESEM images of nanostructures fabricated with different molar ratio of Zn and Sn in mixed precursor solution before thermal annealing **(A)** 13Z7S, **(B)** 14Z6S, **(C)** 15Z5S, **(D)** 16Z4S, and **(E)** 17Z3S, and after thermal annealing at 350°C for 1 h **(F)** 13Z7S, **(G)** 14Z6S, **(H)** 15Z5S, **(I)**16Z4S, and **(J)** 17Z3S.

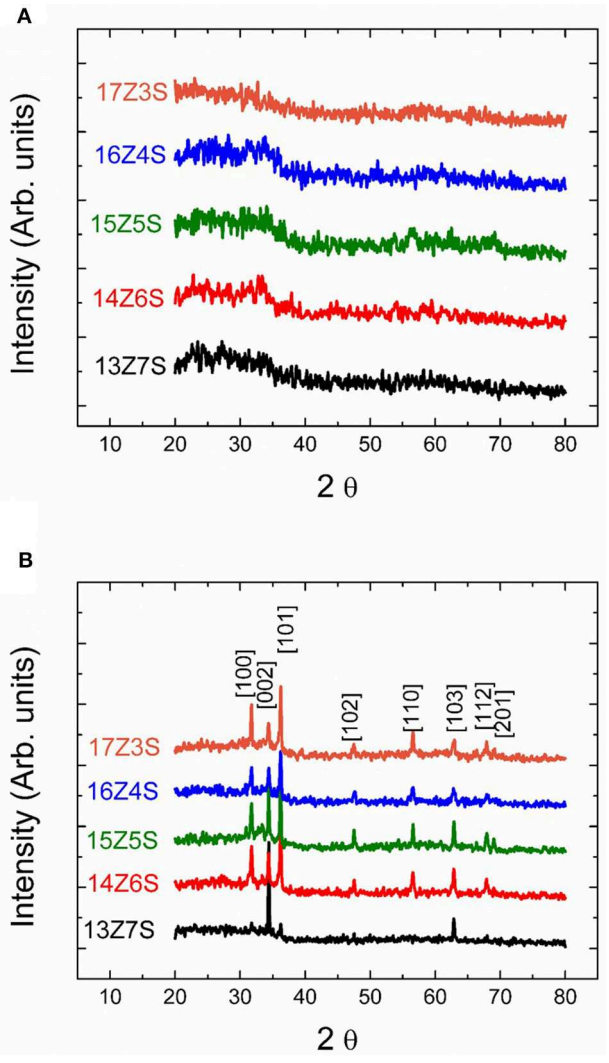

FIGURE 2 | The XRD patterns of ZnO/SnO_2 nanostructures **(A)** before thermal annealing (as-sprayed) and **(B)** after thermal annealing at 350°C.

Similar morphology was reported for film sprayed using $SnCl_4$ precursor solution at spray temperature of 450°C (Korotcenkov et al., 2001; Korotcenkov and Cho, 2009). The films after thermal treatment show different morphology. This morphology tends to contain hexagonal shaped nanostructures. Hexagonal nanocrystals are observed in **Figure 1F** when the molar ratio of Zn:Sn in precursor solution is 13:7, while for values above 13:7, the microstructural feature changes from nanocrystals to nanorods (**Figures 1G–I**).

The size of the hexagonal nanocrystal is measured within the range of 52–210 nm for 13Z7S film and 43–85 nm for 17Z3S composite film, while the aspect ratio of nanorods (length divided by width) is calculated as 4.5 (length $l = 450$ nm and diameter $d = 100$ nm), 5.2 ($l = 650$ nm, $d = 125$ nm), and 3 ($l = 1200$ nm, $d = 400$ nm), for 14Z6S, 15Z5S, and 16Z4S films, respectively. As we reported earlier, high aspect ratio of ZnO nanorods was observed when the mass ratio of Zn:Sn in the precursor solution was 3:1. Here, similar result with dense structure is obtained for 15Z5S film after thermal annealing (**Figure 1H**) when optimize the growth of ZnO by changing various molar ratio of Zn/Sn in the precursor mixture. The nanorod-like nanostructures start to disappear when the Zn:Sn molar ratio is 13:7 and lower. These also seem to disappear when the ratio is 17:3 and higher. The compact film and porous film like structure are obtained when the molar ratio of Zn:Sn in precursor solution is 12:8 and 18:2, respectively (**Supplementary Figure 1**).

XRD Analysis

The crystal structure of sprayed thin films before and after thermal annealing at 350°C is investigated by X-ray diffractometer and the patterns are shown in **Figure 2**. No sharp peaks are observed in the unannealed films regardless of the molar ratio of Zn to Sn in the precursor solution (**Figure 2A**). This indicates that the films are amorphous in nature before thermal annealing. However, sharp diffraction peaks corresponding to ZnO are observed in the sprayed mixed films after thermal annealing at 350°C for 1 h (**Figure 2B**), demonstrating the formation of well-crystalline ZnO nanorod. This indicates that the crystalline structures formed during the thermal annealing process. Formation of crystalline structures during thermal annealing is also supported by FESEM with the presence of nanostructures in the films after thermal treatment. The diffraction peaks in **Figure 2B** at 2θ values of 32, 34, 36, 47.5, 56, 63, 68, and 69 degree can be indexed as (100), (002), (101), (102), (110), (103), (112), and (201) crystal planes of the hexagonal wurtzite structure of ZnO (JCPDS No. 79-0208). The XRD pattern of 13Z7S film shows weak ZnO peaks compared to other XRD patterns observed for various Zn/Sn ratio. This is due to low amount of zinc precursor used in the mixture of Zn:Sn = 13:7 as compared to high amount of zinc used in the mixture of Zn:Sn = 17:3. The intensity of XRD peaks is increasing with increase of Zn precursor in the mixture. Interestingly there are no pronounced peaks corresponding to SnO_2 observed in any of the annealed mixed thin film. However,

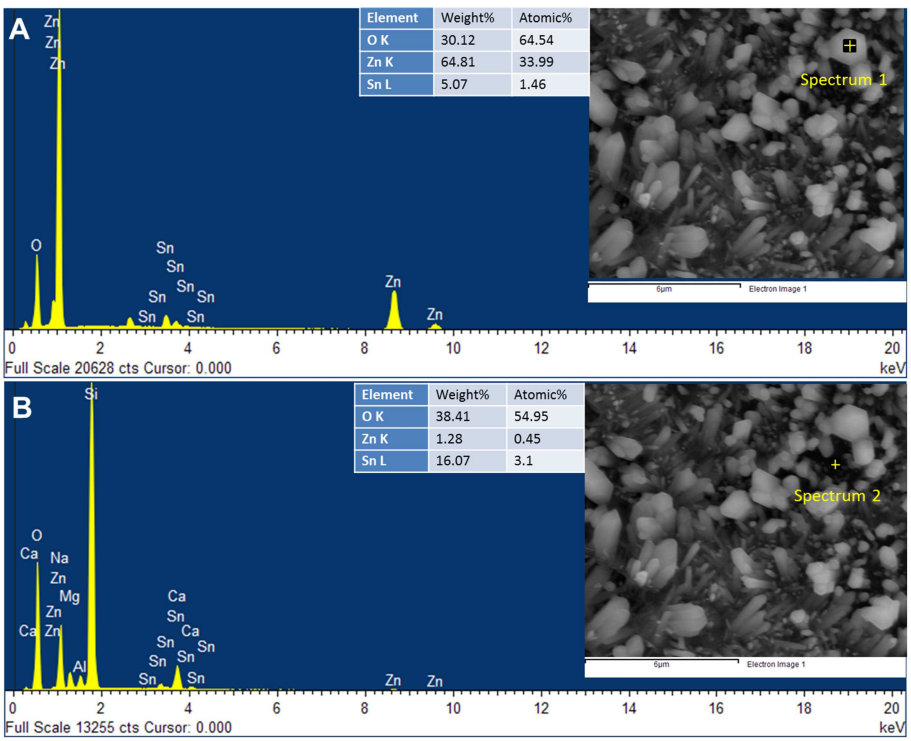

FIGURE 3 | The EDX spectra obtained at two different positions: **(A)** on the ZnO nanorod and **(B)** on the surface of the 15Z5S film.

the EDX measurement shows that nanorods are composed of ZnO, while the underlying film contains significant amount of Sn as shown in **Figure 3B**. This can be attributed to the presence of amorphous SnO_2 in the film. It is reported that the crystallization temperature of spray deposited SnO_2 films are above 500°C. Patil et al. (2011) reported that the sprayed films baked at 550°C shows very small peaks corresponding SnO_2, indicating their predominantly amorphous nature. So, it is suggested that the SnO_2 remains amorphous at 350°C which is considerably lower than the crystallization temperature of SnO_2. On the other hand, researchers reported that the crystallization temperature of ZnO films was 350°C or lower (Cho et al., 1999; Lee et al., 2004). From the FESEM images and XRD spectra, we can conclude that the films contain crystalline ZnO nanostructures and amorphous SnO_2 underlying film.

EDX spectrum obtained on the nanorod of the 15Z5S film shows that nanorods are composed of ZnO (**Figure 3A**), while less amount of Sn is detected. It may arise due to deep penetration of EDX beam and probing the underlying film. However, the EDX spectrum obtained on the surface of the 15Z5S film (**Figure 3B**) reveals the underlying film contains significant amount of Sn, while peaks for Si, Ca, Al, Na, and Mg are detected from the substrate.

Ethanol Sensing Properties

The fabricated ZnO/SnO_2 nanostructures are then tested for ethanol sensing at an optimum operating temperature of 400°C. Pure ZnO and SnO_2 thin films are also studied for comparison with the ZnO/SnO_2 nanostructures sensors toward ethanol. **Figure 4A** illustrates the sensitivity of sensors to ethanol at different concentrations from 25 to 400 ppm. As clearly seen in **Figure 4A**, the gas sensing performances of ZnO/SnO_2 nanostructures are exceptionally high when compared to pure ZnO and SnO_2 thin film sensors. Sensitivity of ethanol first

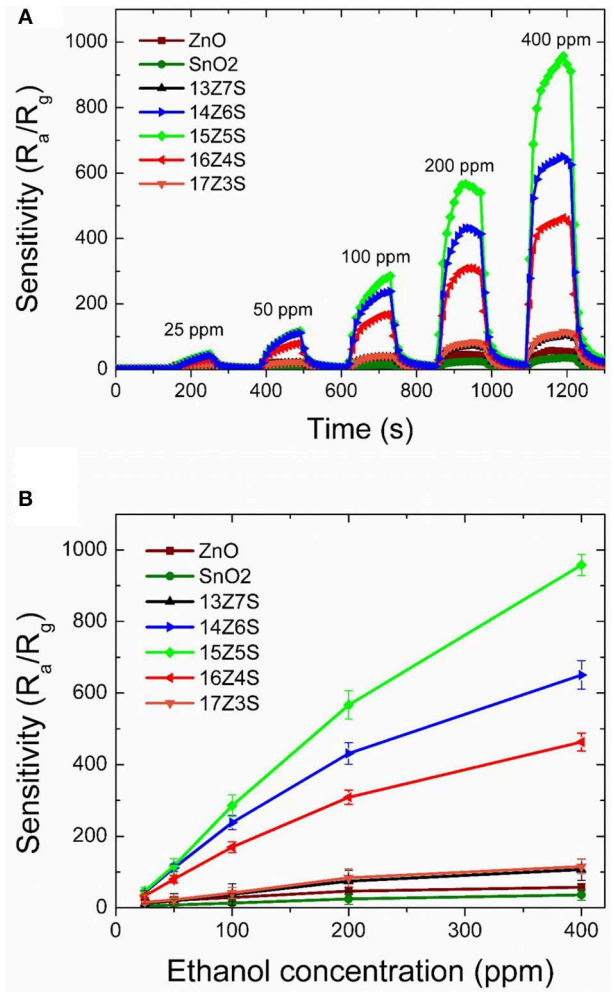

FIGURE 4 | (A) Time-dependent response recovery characteristics of various ZnO/SnO_2 nanostructure sensors with different gas concentrations at an optimum operating temperature of 400°C, **(B)** Sensitivity of various ZnO/SnO_2 nanostructure sensors as a function of ethanol concentrations.

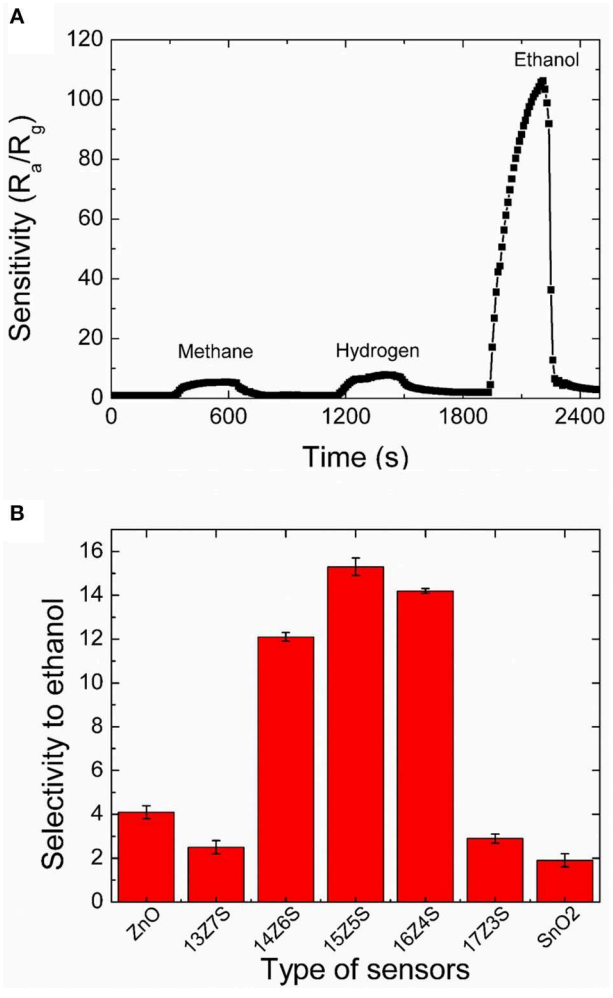

FIGURE 5 | (A) Selectivity of 15Z5S film sensors toward 50 ppm of methane, hydrogen and ethanol at an operating temperature of 400°C and **(B)** the variation of selectivity (ratio between the sensitivity of 50 ppm ethanol and hydrogen at 400°C) of the sensors fabricated with different films.

rises as the molar ratio of Zn/Sn in the film increases from 13:7 to 15:5 which corresponds to the films 13Z7S, 14Z6S, and 15Z5S. Sensitivity then decreases when the molar ratio of Zn/Sn increases beyond the limit of 15:5 (16Z4S and 17Z3S). It can be seen from **Figure 4A** that sensitivities toward an ethanol concentration of 25 ppm are about 4, 5, 12, 42, 50, 33, and 16 for pure SnO_2, pure ZnO, 13Z7S, 14Z6S, 15Z5S, 16Z4S, and 17Z3S nanostructure film sensors, respectively. 15Z5S film sensor exhibits highest sensitivity toward ethanol among other sensors. The enhancement of the ethanol sensing performance of 15Z5S nanostructured film can be attributed to the greater sensing surface area due to the high aspect ratio of nanorod structure. Sensitivity as a function of ethanol concentration is shown in **Figure 4B**. The sensitivity toward ethanol gas increases linearly up to 200 ppm concentration for all film sensors. Beyond 200 ppm concentration, the sensitivity tends to reach saturation gradually after climbing over the point of 400 ppm concentration. But, 15Z5S sensor exhibits linear ethanol sensing property as compared to other sensors. Further, these sensors exhibit the lowest detection limit for ethanol as 25 ppm. As can be seen the sensitivity of 15Z5S nanostructure film sensors for ethanol is almost ten times higher than that of the pure sensors for 25 ppm of ethanol concentration.

Thermodynamic analysis reveals that methane and hydrogen are formed from ethanol at moderate temperatures and high temperatures (400–700°C), respectively (Vasudeva et al., 1996; Fishtik et al., 2000; Galvita et al., 2001). Therefore, selective ethanol sensing is important in presence of hydrogen and methane. Thus, the selectivity of the 15Z5S film sensor toward ethanol is studied. **Figure 5A** represents the continuous response of 15Z5S film to 50 ppm methane, hydrogen and ethanol. The 15Z5S sensor reveals sensitivity of 5 to methane, 7 to hydrogen, and 108 to ethanol. The sensitivity of 108 is obtained for ethanol for the 15Z5S film sensor which is nearly 15-fold higher than that of the response for methane and hydrogen at an operating temperature of 400°C. **Figure 5B** summarizes the selectivity of ethanol in terms of the sensing ratios of ethanol and hydrogen which produced the second largest sensing signal in all sensors regardless of Zn:Sn ratio. Thus, the 15Z5S film shows better selectivity toward ethanol than the other mixed thin films sensor which is higher than that of the pure ZnO and SnO_2 film sensors due to the one-dimensional nanostructure (nanorod) nature with high sensing surface area. Therefore, 15Z5S nanostructure film-based sensor can be used to detect ethanol in practical applications in the environmental field.

Gas Sensing Mechanism

The detailed sensing mechanism of ZnO nanorod on SnO_2 thin film is shown in **Figure 6**. It is commonly accepted that the sensing of a reducing gas in a metal oxide surface at elevated temperature is a two-step process which includes the formation of oxygen ion species on the surface and reducing gases are oxidized on the surface (Barsan and Weimar, 2001; Kolmakov et al., 2003). Due to variation of band gap, work function and electron affinity of ZnO and SnO_2 a Fermi electron transfer is possible at the ZnO/SnO_2 interface (Zheng et al., 2009). Thus, a net electron flow from SnO_2 to ZnO can be expected at the ZnO/SnO_2 interface which is mainly due to the difference in work functions of ZnO (5.2 eV) and SnO_2 (4.9 eV) (Tang et al., 2014; Li et al., 2015). This increases the electron density at the ZnO nanorods and the underlying SnO_2 layer will suffer from an electron deficiency (**Figure 6A**).

When the sensor is exposed to air at elevated temperature, due to the increased electron density at ZnO nanostructures, the amount of oxygen ions (O^{2-}) present in the ZnO surface also increases. At operating temperature of 400°C, the O^{2-} ions are more stable and predominant when compared to other oxygen species such as (O^-, O_2^-) (Barsan and Weimar, 2001; Yao et al., 2014) (**Figure 6B**). When the sensor is exposed to ethanol, the surface oxygen species reacts with the ethanol molecules and the chemisorbed electrons will be left freely to the films (**Figure 6C**).

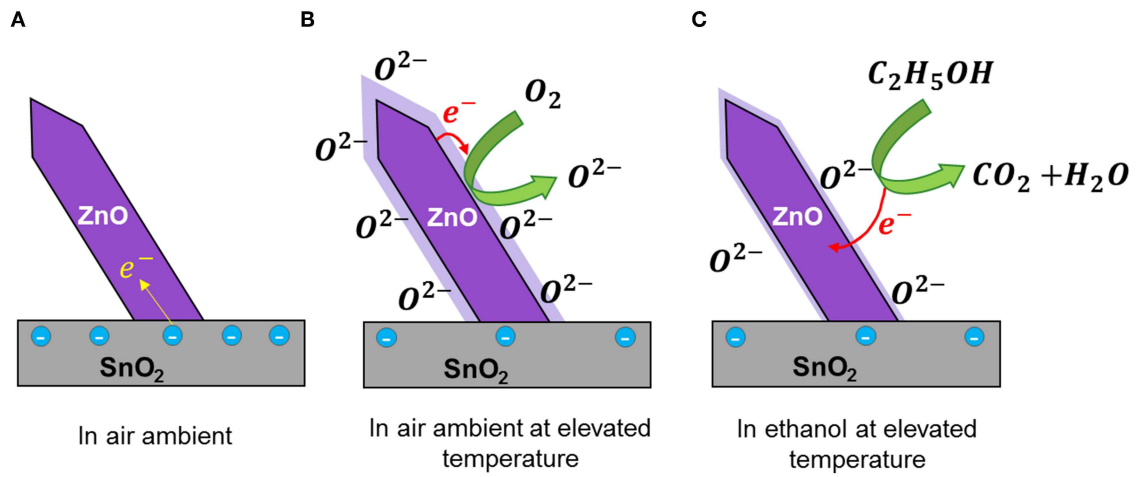

FIGURE 6 | Schematic ethanol sensing mechanism of ZnO nanorod on SnO_2 thin film **(A)** In air ambient, **(B)** In air ambient at elevated temperature, and **(C)** In ethanol at elevated temperature.

TABLE 2 | Brief summary of ZnO/SnO_2 nanostructures gas sensor upon exposure to 100 ppm ethanol.

ZnO/SnO_2 nanostructures	Fabrication method	Detection range (ppm)	Sensitivity**	Working temperature (°C)	References
ZnO/SnO_2 nanostructures	Hydrothermal	10–1,000	30	300	Li et al., 2011
ZnO/SnO_2 hollow nanospheres	Hydrothermal	0.5–100	78.2	225	Liu et al., 2017
SnO_2- core/ZnO-shell nanowires	Thermal evaporation and Spray coating*	25–500	14.05	400	Thanh Le et al., 2013
ZnO/SnO_2 hollow nanospheres	Hydrothermal*	10–500	14.7	150	Ma et al., 2013
SnO_2/ZnO nanofibers	Electrospinning and Hydrothermal*	5–1,000	80	300	Yan et al., 2015a
Hollow ZnO/SnO_2 nanofibers	Electrospinning and Hydrothermal*	5–1,000	392.29	200	Li et al., 2015
ZnO sphere and SnO_2 nanofiber composite	Electrospinning and Hydrothermal*	20 ppm	100 (for 20ppm)	210	Guo and Wang, 2016
SnO_2/ZnO hetero-nanofibers	Electrospinning	5–1,000	54	300	Yan et al., 2015b
Ag-doped ZnO-SnO_2 hollow nanofiber	Electrospinning and Hydrothermal*	1–6,000	128.6	200	Ma et al., 2017
ZnO-nanorod/SnO_2 thin film	Spray pyrolysis	20–400	285	400	This work

The methods are 2-step process for each metal oxide.

***Sensitivity for 100 ppm ethanol at optimum temperature unless mentioned.*

As a result, a rapid drop in net resistance of the film was observed. Therefore, sensitivity is increased toward ethanol.

According to the sensing results, 15Z5S nanostructure film sensor exhibits maximum ethanol sensing properties compared with pure ZnO, pure SnO_2, and other mixed thin films (13Z7S, 14Z6S, 16Z4S, and 17Z3S). The improved sensitivity of 15Z5S film sensor with high aspect ratio nanorods for ethanol than the pure and other mixed thin film sensor can be feasibly explained by highly crystalline ZnO nanorods, which improve the effective sensing surface with improved surface oxygen species density. Ethanol sensing results of our ZnO-nanorod/SnO_2-thinfilm (15Z5S) sensor is compared with the previous reported values. **Table 2** summarizes the ethanol sensing properties of ZnO/SnO_2 composite gas sensors. It clearly shows that the sensitivity of our ZnO-nanorod/SnO_2-thinfilm (15Z5S) sensor is comparable to some of the recent works with relatively simple and low-cost fabrication techniques and exhibits greater sensitivity toward ethanol. Therefore, the present ethanol sensor can be used to detect ethanol in environmental monitoring.

CONCLUSIONS

We report a simple spray pyrolysis and heating route to fabricate ZnO nanorod on SnO_2 thin film with controllable morphologies. The nanostructures are tailored by controlling the Zn:Sn ion ratio in the precursor solution. The resulting nanostructures turns into high aspect ratio nanorods when the Zn:Sn ratio is 15:5. The ethanol sensing studies reveals that the mixed films perform well when compared to pure ZnO and SnO_2 films. The sensitivity of 108 is obtained for 50 ppm ethanol from ZnO-nanorod/SnO_2-thinfilm (15Z5S) sensor which is nearly 15-fold higher than that of the response for methane and hydrogen at an operating temperature of 400°C. Also, the ZnO nanorod on the SnO_2 thin film sensor shows better sensitivity and selectivity toward ethanol due to high aspect ratio of nanorod structure with greater sensing surface area than film.

AUTHOR CONTRIBUTIONS

TT conducted all the experimental work and analyzed the data. MT and TT wrote the manuscript with the guidance of SA and AH. SA guided the sensing part of this work and corrected the manuscript. AH directed the fabrication part of ZnO nanorod on SnO_2 film and supervised the manuscript writing.

ACKNOWLEDGMENTS

Authors acknowledge University of Malaya and Ministry of Higher Education, Malaysia for its financial assistance for this research work under FRGS Grant (FP014-2015A). SA work was supported by the National Science Foundation Grant 1609142.

SUPPLEMENTARY MATERIAL

The Supplementary Material for this article can be found online at: https://www.frontiersin.org/articles/10.3389/fmats.2019.00122/full#supplementary-material

Supplementary Figure S1 | FESEM images of 12Z8S and 18Z2S thinfilms before **(a)**, **(c)** and after **(b)**, **(d)** heating at 350C for 1 hour.

REFERENCES

Amma, D. S. D., Vaidyan, V. K., and Manoj, P. K. (2005). Structural, electrical and optical studies on chemically deposited tin oxide films from inorganic precursors. *Mater. Chem. Phys.* 93, 194–201. doi: 10.1016/j.matchemphys.2005.03.045

Andre, R. S., Mercante, L. A., Facure, M. H. M., Mattoso, L. H. C., and Correa, D. S. (2019). Enhanced and selective ammonia detection using In 2 O 3 /reduced graphene oxide hybrid nanofibers. *Appl. Surf. Sci.* 473, 133–140. doi: 10.1016/j.apsusc.2018.12.101

Arafat, M. M., Haseeb, A. S. M. A., and Akbar, S. A. (2014). "Developments in semiconducting oxide-based gas-sensing materials,"

in *Comprehensive Materials Processing* (Elsevier), 205–219. doi: 10.1016/B978-0-08-096532-1.01307-8

Barsan, N., and Weimar, U. (2001). Conduction model of metal oxide gas sensors. *J. Electroceramics* 7, 143–167. doi: 10.1023/A:1014405811371

Chen, X., Deng, N., Zhang, X., Li, J., Yang, Y., Hong, B., et al. (2019). Cerium-doped indium oxide nanosphere arrays with enhanced ethanol-sensing properties. *J. Nanoparticle Res.* 21:77. doi: 10.1007/s11051-019-4516-3

Cheng, C., Liu, B., Yang, H., Zhou, W., Sun, L., Chen, R., et al. (2009). Hierarchical assembly of ZnO nanostructures on SnO $_2$ backbone nanowires: low-temperature hydrothermal preparation and optical properties. *ACS Nano* 3, 3069–3076. doi: 10.1021/nn900848x

Cho, S., Ma, J., Kim, Y., Sun, Y., Wong, G. K. L., and Ketterson, J. B. (1999). Photoluminescence and ultraviolet lasing of polycrystalline ZnO thin films prepared by the oxidation of the metallic Zn. *Appl. Phys. Lett.* 75, 2761–2763. doi: 10.1063/1.125141

Comini, E., Ferroni, M., Guidi, V., Faglia, G., Martinelli, G., and Sberveglieri, G. (2002). Nanostructured mixed oxides compounds for gas sensing applications. *Sens. Actu. B Chem.* 84, 26–32. doi: 10.1016/S0925-4005(02)00006-0

Demir-Cakan, R., Hu, Y.-S. S., Antonietti, M., Maier, J., and Titirici, M.-M. M. (2008). Facile one-pot synthesis of mesoporous SnO 2 microspheres via nanoparticles assembly and lithium storage properties. *Chem. Mater.* 20, 1227–1229. doi: 10.1021/cm7031288

Dey, A. (2018). Semiconductor metal oxide gas sensors: a review. *Mater. Sci. Eng. B Solid-State Mater. Adv. Technol.* 229, 206–217. doi: 10.1016/j.mseb.2017.12.036

Drobek, M., Kim, J. H., Bechelany, M., Vallicari, C., Julbe, A., and Kim, S. S. (2016). MOF-based membrane encapsulated ZnO nanowires for enhanced gas sensor selectivity. *ACS Appl. Mater. Interfaces* 8, 8323–8328. doi: 10.1021/acsami.5b12062

Fishtik, I., Alexander, A., Datta, R., and Geana, D. (2000). Thermodynamic analysis of hydrogen production by steam reforming of ethanol via response reactions. *Int. J. Hydrogen Energy* 25, 31–45. doi: 10.1016/S0360-3199(99)00004-X

Freitas, J. G., Fletcher, B., Aravena, R., and Barker, J. F. (2010). Methane production and isotopic fingerprinting in ethanol fuel contaminated sites. *Ground Water* 48, 844–857. doi: 10.1111/j.1745-6584.2009.00665.x

Galvita, V. V., Semin, G. L., Belyaev, V. D., Semikolenov, V. A., Tsiakaras, P., and Sobyanin, V. A. (2001). Synthesis gas production by steam reforming of ethanol. *Appl. Catal. A Gen.* 220, 123–127. doi: 10.1016/S0926-860X(01)00708-6

Guo, W., and Wang, Z. (2016). Composite of ZnO spheres and functionalized SnO2nanofibers with an enhanced ethanol gas sensing properties. *Mater. Lett.* 169, 246–249. doi: 10.1016/j.matlet.2016.01.118

He, M., Xie, L., Zhao, X., Hu, X., Li, S., and Zhu, Z. G. (2019). Highly sensitive and selective H 2 S gas sensors based on flower-like WO 3 /CuO composites operating at low/room temperature. *J. Alloys Compd.* 788, 36–43. doi: 10.1016/j.jallcom.2019.01.349

Kolmakov, A., Zhang, Y., Cheng, G., and Moskovits, M. (2003). Detection of CO and O2 using tin oxide nanowire sensors. *Adv. Mater.* 15, 997–1000. doi: 10.1002/adma.200304889

Korotcenkov, G., Brinzari, V., Schwank, J., DiBattista, M., and Vasiliev, A. (2001). Peculiarities of SnO2 thin film deposition by spray pyrolysis for gas sensor application. *Sensors Actuators B Chem.* 77, 244–252. doi: 10.1016/S0925-4005(01)00741-9

Korotcenkov, G., and Cho, B. K. (2009). Thin film SnO2-based gas sensors: film thickness influence. *Sensors Actuators B Chem.* 142, 321–330. doi: 10.1016/j.snb.2009.08.006

Kwak, C. H., Kim, T. H., Jeong, S. Y., Yoon, J. W., Kim, J. S., and Lee, J. H. (2018). Humidity-independent oxide semiconductor chemiresistors using terbium-doped SnO 2 yolk-shell spheres for real-time breath analysis. *ACS Appl. Mater. Interfaces* 10, 18886–18894. doi: 10.1021/acsami.8b04245

Lee, J. H., Yeo, B. W., and Park, B. O. (2004). Effects of the annealing treatment on electrical and optical properties of ZnO transparent conduction films by ultrasonic spraying pyrolysis. *Thin Solid Films* 457, 333–337. doi: 10.1016/j.tsf.2003.09.075

Li, B., Liu, J., Liu, Q., Chen, R., Zhang, H., Yu, J., et al. (2019). Core-shell structure of ZnO/Co 3 O 4 composites derived from bimetallic-organic frameworks with superior sensing performance for ethanol gas. *Appl. Surf. Sci.* 475, 700–709. doi: 10.1016/j.apsusc.2018.12.284

Li, C. C., Yin, X. M., Li, Q. H., and Wang, T. H. (2011). Enhanced gas sensing properties of ZnO/SnO2 hierarchical architectures by glucose-induced attachment. *CrystEngComm* 13, 1557–1563. doi: 10.1039/C0CE00244E

Li, W., Ma, S., Li, Y., Yang, G., Mao, Y., Luo, J., et al. (2015). Enhanced ethanol sensing performance of hollow ZnO-SnO2core-shell nanofibers. *Sensors Actuators B Chem.* 211, 392–402. doi: 10.1016/j.snb.2015.01.090

Lin, Y., Wei, W., Li, Y., Li, F., Zhou, J., Sun, D., et al. (2015). Preparation of Pd nanoparticle-decorated hollow SnO_2 nanofibers and their enhanced formaldehyde sensing properties. *J. Alloys Compd.* 651, 690–698. doi: 10.1016/j.jallcom.2015.08.174

Liu, D., Pan, J., Tang, J., Liu, W., Bai, S., and Luo, R. (2019a). Ag decorated SnO2 nanoparticles to enhance formaldehyde sensing properties. *J. Phys. Chem. Solids* 124, 36–43. doi: 10.1016/j.jpcs.2018.08.028

Liu, J., Wang, T., wang, B., Sun, P., Yang, Q., Liang, X., et al. (2017). Highly sensitive and low detection limit of ethanol gas sensor based on hollow ZnO/SnO_2 spheres composite material. *Sensors Actuators B Chem.* 245, 551–559. doi: 10.1016/j.snb.2017.01.148

Liu, S., Sun, Q., Wang, J., and Hou, H. (2019b). Charge imbalance induced oxygen-adsorption enhances the gas-sensing properties of Al-doped SnO 2 powders. *J. Phys. Chem. Solids* 124, 163–168. doi: 10.1016/j.jpcs.2018.09.017

Lu, G., Xu, J., Sun, J., Yu, Y., Zhang, Y., and Liu, F. (2012). UV-enhanced room temperature NO2sensor using ZnO nanorods modified with SnO2nanoparticles. *Sensors Actuators B Chem.* 162, 82–88. doi: 10.1016/j.snb.2011.12.039

Lupan, O., Postica, V., Gröttrup, J., Mishra, A. K., de Leeuw, N. H., and Adelung, R. (2017). Enhanced UV and ethanol vapour sensing of a single 3-D ZnO tetrapod alloyed with Fe2O3nanoparticles. *Sensors Actuators B Chem.* 245, 448–461. doi: 10.1016/j.snb.2017.01.107

Ma, L., Ma, S.Y., Kang, H., Shen, X. F., Wang, T. T., Jiang X. H., et al. (2017). Preparation of Ag-doped ZnO-SnO_2 hollow nanofibers with an enhanced ethanol sensing performance by electrospinning. *Mater. Lett.* 209, 188–192. doi: 10.1016/j.matlet.2017.08.004

Ma, X., Song, H., and Guan, C. (2013). Enhanced ethanol sensing properties of ZnO-doped porous SnO2 hollow nanospheres. *Sensors Actuators B Chem.* 188, 193–199. doi: 10.1016/j.snb.2013.06.099

Miller, D. R., Akbar, S. A., and Morris, P. A. (2014). Nanoscale metal oxide-based heterojunctions for gas sensing: a review. *Sensors Actuators B Chem.* 204, 250–272. doi: 10.1016/j.snb.2014.07.074

NaderiNasrabadi, M., Mortazavi, Y., and Khodadadi, A. A. (2016). Highly sensitive and selective Gd2O3-doped SnO2 ethanol sensors synthesized by a high temperature and pressure solvothermal method in a microreactor. *Sensors Actuators B Chem.* 230, 130–139. doi: 10.1016/j.snb.2016.02.045

Pan, K. Y., Lin, Y. H., Lee, P. S., Wu, J. M., and Shih, H. C. (2012). Synthesis of SnO 2-ZnO core-shell nanowires and their optoelectronic properties. *J. Nanomater.* 2012, 1–6. doi: 10.1155/2012/279245

Park, S., An, S., Mun, Y., and Lee, C. (2013). UV-Enhanced NO $_2$ gas sensing properties of SnO_2 -core/ZnO-shell nanowires at room temperature. *ACS Appl. Mater. Interfaces* 5, 4285–4292. doi: 10.1021/am400500a

Park, S., Kim, S., Sun, G. J., and Lee, C. (2015). Synthesis, structure, and ethanol gas sensing properties of In_2O_3 nanorods decorated with Bi_2O_3 nanoparticles. *ACS Appl. Mater. Interfaces* 7, 8138–8146. doi: 10.1021/acsami.5b00972

Patil, G. E., Kajale, D. D., Chavan, D. N., Pawar, N. K., Ahire, P. T., Shinde, S. D., et al. (2011). Synthesis, characterization and gas sensing performance of SnO_2 thin films prepared by spray pyrolysis. *Bull. Mater. Sci.* 34, 1–9. doi: 10.1007/s12034-011-0045-0

Powers, S. E., Hunt, C. S., Heermann, S. E., Corseuil, H. X., Rice, D., and Alvarez, P. J. J. (2001). The transport and fate of ethanol and BTEX in groundwater contaminated by gasohol. *Crit. Rev. Environ. Sci. Technol.* 31, 79–123. doi: 10.1080/20016491089181

Rong, P., Ren, S., and Yu, Q. (2019). Fabrications and applications of ZnO nanomaterials in flexible functional devices-a review. *Crit. Rev.Anal. Chem.* 49, 333–349. doi: 10.1080/10408347.2018.1531691

Sakthivel, B., and Nammalvar, G. (2019). Selective ammonia sensor based on copper oxide/reduced graphene oxide nanocomposite. *J. Alloys Compd.* 788, 422–428. doi: 10.1016/j.jallcom.2019.02.245

Tan, W., Tan, J., Fan, L., Yu, Z., Qian, J., and Huang, X. (2018). Fe2O3-loaded NiO nanosheets for fast response/recovery and high response gas sensor. *Sensors Actuators B Chem.* 256, 282–293. doi: 10.1016/j.snb.2017.09.187

Tang, W., Wang, J., Yao, P., and Li, X. (2014). Hollow hierarchical SnO2-ZnO composite nanofibers with heterostructure based on electrospinning method for detecting methanol. *Sensors Actuators B Chem.* 192, 543–549. doi: 10.1016/j.snb.2013.11.003

Thanh Le, D. T., Trung, D. D., Chinh, N. D., Thanh Binh, B. T., Hong, H. S., Van Duy, N., et al. (2013). Facile synthesis of SnO2-ZnO core-shell nanowires for enhanced ethanol-sensing performance. *Curr. Appl. Phys.* 13, 1637–1642. doi: 10.1016/j.cap.2013.06.024

Tharsika, T., Haseeb, A. S. M. A., and Sabri, M. F. M. (2014a). Photoluminescence studies on spray pyrolysis deposited ZnO-SnO2 mixed thin films. *Adv. Mater. Res.* 25, 318–322. doi: 10.4028/www.scientific.net/AMR.925.318

Tharsika, T., Haseeb, A. S. M. A., and Sabri, M. F. M. (2014b). Structural and optical properties of ZnO-SnO2mixed thin films deposited by spray pyrolysis. *Thin Solid Films* 558, 283–288. doi: 10.1016/j.tsf.2014.02.022

Tharsika, T., Haseeb, A. S. M. A. S. M. A., Akbar, S. A. A., and Thanihaichelvan, M. (2015). Tailoring ZnO nanostructures by spray pyrolysis and thermal annealing. *Ceram. Int.* 41, 5205–5211. doi: 10.1016/j.ceramint.2014.12.062

Timmer, B., Olthuis, W., and Van Den Berg, A. (2005). Ammonia sensors and their applications—A review. *Sensors Actuators B Chem.* 107, 666–677. doi: 10.1016/j.snb.2004.11.054

ul Haq, M., Zhang, Z., Wen, Z., Khan, S., ud Din, S., Rahman, N., et al. (2019). Humidity sensor based on mesoporous Al-doped NiO ultralong nanowires with enhanced ethanol sensing performance. *J. Mater. Sci. Mater. Electron.* 30, 1–14. doi: 10.1007/s10854-019-01030-8

Vasudeva, K., Mitra, N., Umasankar, P., and Dhingra, S. C. (1996). Steam reforming of ethanol for hydrogen production: thermodynamic analysis. *Int. J. Hydrogen Energy* 21, 13–18. doi: 10.1016/0360-3199(95)00030-H

Wang, H., and Rogach, A. L. (2014). Hierarchical SnO2 nanostructures: recent advances in design, synthesis, and applications. *Chem. Mater.* 26, 123–133. doi: 10.1021/cm4018248

Wang, Q., Bai, J., Huang, B., Hu, Q., Cheng, X., Li, J., et al. (2019). Design of $NiCo_2O_4$@SnO_2 heterostructure nanofiber and their low temperature ethanol sensing properties. *J. Alloys Compd.* 791, 1025–1032. doi: 10.1016/j.jallcom.2019.03.364

Wang, T., Xu, S., Hu, N., Hu, J., Huang, D., Jiang, W., et al. (2018). Microwave preparation and remarkable ethanol sensing properties of ZnO particles with controlled morphologies in water-ethylene glycol binary solvent system. *Sensors Actuators B Chem.* 255, 1006–1014. doi: 10.1016/j.snb.2017.08.099

Yan, S. H., Ma, S. Y., Li, W. Q., Xu, X. L., Cheng, L., Song, H. S., et al. (2015a). Synthesis of SnO2-ZnO heterostructured nanofibers for enhanced ethanol gas-sensing performance. *Sensors Actuators B Chem.* 221, 88–95. doi: 10.1016/j.snb.2015.06.104

Yan, S. H., Ma, S. Y., Xu, X. L., Li, W. Q., Luo, J., Jin, W. X., et al. (2015b). Preparation of SnO_2–ZnO hetero-nanofibers and their application in acetone sensing performance. *Mater. Lett.* 159, 447–450. doi: 10.1016/j.matlet.2015.07.051

Yang, X., Yu, Q., Zhang, S., Sun, P., Lu, H., Yan, X., et al. (2018). Highly sensitive and selective triethylamine gas sensor based on porous SnO2/Zn2SnO4 composites. *Sensors Actuators B Chem.* 266, 213–220. doi: 10.1016/j.snb.2018.03.044

Yao, M., Ding, F., Cao, Y., Hu, P., Fan, J., Lu, C., et al. (2014). Sn doped ZnO layered porous nanocrystals with hierarchical structures and modified surfaces for gas sensors. *Sensors Actuators B Chem.* 201, 255–265. doi: 10.1016/j.snb.2014.04.078

Yao, M.-S., Tang, W.-X., Wang, G.-E., Nath, B., and Xu, G. (2016). MOF thin film-coated metal oxide nanowire array: significantly improved chemiresistor sensor performance. *Adv. Mater.* 28, 5229–5234. doi: 10.1002/adma.201506457

Zheng, L., Zheng, Y., Chen, C., Zhan, Y., Lin, X., Zheng, Q., et al. (2009). Network structured SnO_2/ZnO heterojunction nanocatalyst with high photocatalytic activity. *Inorg. Chem.* 48, 1819–1825. doi: 10.1021/ic802293p

Conflict of Interest Statement: The authors declare that the research was conducted in the absence of any commercial or financial relationships that could be construed as a potential conflict of interest.